JOURNAL OF PROPULSION AND POWER
Vol. 25, No. 3, May–June 2009

Flow Characteristics of Tip Injection on Compressor Rotating Spike via Time-Accurate Simulation

Jen-Ping Chen* and Benjamin Johnson†
The Ohio State University, Columbus, Ohio 43021
Michael D. Hathaway‡
U.S. Army Research Laboratory, Cleveland, Ohio 44135
and
Robert S. Webster§
University of Tennessee, Chattanooga, Tennessee 37403

DOI: 10.2514/1.41428

The performance of gas turbine engines is often limited by compressor stall. Steady tip-injection stall control technologies have demonstrated their effectiveness to increase the stable operating range of gas turbine engine compressors. To help understand the fluid mechanic processes of stall with and without stall control and how stall is mitigated by stall control technology, the establishment of a capability to simulate the flow details leading to stall would be extremely helpful. This paper presents results of the simulations of a high-speed single-stage axial compressor. These simulations show the evolution of rotating spikes and range extension as a result of tip injection. The simulations are time-accurate simulations of the three-dimensional Navier–Stokes equations encompassing the full-annulus grid and are executed using high-performance parallel computing. Computed compressor characteristics are compared to experimental data. The general flow features of the compressor with and without tip injection at the onset of stall are presented using time-accurate pressure traces and visualized using a novel disturbance cell concept.

I. Introduction

ROTATING stall control technologies have been demonstrated to extend the stable operating range of axial compressors [1–6]. Upstream of a compressor rotor, high total pressure (relative to the rotor) air is injected at discrete locations through the casing into the rotor tip region. This injected air alters the three-dimensional flowfield above the rotor tip causing the clearance flow to move aft in the rotor passage locally increasing the streamwise momentum (relative to the rotor). This increase in the streamwise momentum is responsible for delaying the onset of rotating stall. Injection not only improves stability margin but also reduces tip losses as the injected jet reduces the blade incidence and therefore partially unloads the rotor tip.

These stability enhancement technologies have been developed through parametric experimental studies. Their effectiveness is based on altering the unsteady flowfield near the compressor blade tips. However, there is a lack of fundamental understanding of the fluid mechanic processes of stall onset and how these stall control technologies mitigate the onset of rotating stall to achieve increased compressor stability. Improved understanding of the stall onset process, with and without tip injection, will guide further development of stall control devices and of compressor blading with increased tolerance to stall, which could lead to an expanded operational envelope of gas turbine engines.

Received 16 October 2008; revision received 8 November 2008; accepted for publication 13 November 2008.

*Associate Professor, Aerospace Engineering, 319B Bolz Hall, 2036 Neil Avenue. Member AIAA.
†Graduate Research Assistant, Aerospace Engineering, 319B Bolz Hall, 2036 Neil Avenue.
‡Aerospace Engineer, Vehicle Technology Directorate, 21000 Brookpark Road, Mail Stop 5-10. Member AIAA.
§Associate Research Professor, UTC SimCenter, 701 East Martin Luther King Boulevard. Member AIAA.

Most of the research on rotating stall has been experimental focusing on understanding its onset. The events leading to rotating stall have been traditionally classified according to two different types of wave disturbances rotating around the annulus: long-length (modal) and short-length (spike) waves [7]. Modal disturbance is associated with the characteristic frequencies of the compression system; the axial length of the disturbance can extend over the entire length of the compressor. Modal disturbances are essentially a two-dimensional phenomenon and they are not an early form of stall cell but instead represent harmonic oscillations of the flowfield. The second form of stall inception is the spike. These are disturbances in which length scale is on the order of a blade passage breadth. Flow instabilities within blade passages initiate the spike disturbances. Spikes can be viewed as embryonic stall cells with flow breakdown in local regions [7]. Spikes are inherently three dimensional whose development depends on the flow structure within the blade passage.

In addition to traditional experimental approaches to understand the development of rotating stall, numerical simulations have been shown to provide another means to shed light on this complicated fluid process. Because of the complex flow structure of the rotating stall, which is characterized by the unsteady, 3-D separated flows, detailed measurement of the flow is difficult if not impossible because of problems with placement and limitation of the measuring devices. Numerical simulation, on the other hand, can provide a higher degree of flow resolution, thus providing deeper insight into the complex flowfield at the onset of stall.

During the last 10 years, steady-flow computational simulations have provided an increasingly accurate prediction of the flow up to the point of compressor stall. Attempts to study stall through unsteady simulations of a subset of the blades in a compressor blade row [8–10] or through reduced-order unsteady flow models [11] have resulted in valuable findings of the flow structure leading to stall. Numerical studies of air injection on compressors were also done with single passage models [1,12,13]. However, because the temporal flowfield variations that occur during stall inception are not necessarily harmonics of blade passing frequency, the unsteady flow in every blade passage within a blade row must be simulated in order to study the transition from a stable flow state to the unstable state at the onset of stall. This is necessary to resolve flow features of the

length scale on the order of the rotor circumference. Such simulations have been done two dimensionally [14,15], but spike instabilities which lead to stall are inherently three-dimensional unsteady phenomena. Modeling the route to stall via a spike instability may require a 3-D unsteady full-annulus simulation, which is a daunting computational endeavor requiring considerable computational resources. Because of the rapid advance of high performance computing in the past decade, advanced computational fluid dynamics codes have benefited from the almost unlimited computing potential of parallel computing. Recently, full-annulus, three-dimensional unsteady computations of a compressor stage [16,17] and an isolated rotor [18] demonstrated the feasibility of using high-performance computing to simulate the development of rotating stall.

In this study the time-evolving development of rotating spike with and without tip injection in a transonic axial compressor is simulated. The simulations are of a full annulus of an axial flow compressor stage. They are three dimensional, and unsteady. The goal of this study was to further the understanding of the onset of rotating stall and its underpinnings. Specifically, this study established a numerical procedure to model the entire flowfield at the onset of rotating spike and a means to analyze the fluid dynamics by which tip injection enhances the operating range of an axial compressor. Compressor speed lines and samples of the unsteady pressure field are presented. The flowfield with tip injection is analyzed in detail. This analysis uses a simple visualization technique to identify disturbance cells that resemble stall cells. Two quantitative measurements, angle of attack and diffusion factor (DF), are correlated with the onset of disturbance cells. Together, these metrics are used as a measure of flow stability and to quantify the impact of tip injection on flow stability.

II. Computational Methodology

The parallel turbomachinery flow solver TURBO [19] was used in this work. The code is a physics-based simulation tool for multistage turbomachinery. It solves the fluid conservation laws without ad hoc modeling of any flow phenomena other than models required for turbulence. This code solves the unsteady Reynolds-averaged Navier–Stokes equations and accounts for turbulence using a k–ε turbulence model. The parallel implementation employs domain decomposition and supports general multiblock grids with arbitrary grid-block connectivity. The solution algorithm is a Newton iterative implicit time-accurate scheme with characteristics-based finite volume spatial discretization. Because all of the fundamental fluid mechanics are computed, the code is capable of capturing the nonlinear characteristics of the flowfields of interest. With the actual modeling of blade rows in relative motion, this code is capable of computing the unsteady interactions between blade rows. Details of the flow solver can be found in [20] and the approach to parallelization for large-scale, complex problems is discussed in [19]. The code has been validated extensively in the past with various compressors and turbines [21–30] and is considered adequate for this study.

III. NASA Stage 35

This transonic compressor stage consists of 36 rotor blades and 46 stator blades (Fig. 1). When running at design speed of 17,194 rpm, it delivers a total pressure ratio of 1.82 at the design flow rate (20.2 kg/s). To facilitate comparison of simulations with and without tip injection, the simulations used a three-blade-row grid as shown in Fig. 2. The grid consists of an injector, rotor, and stator blade row. The injector row has 12 injectors that are equally spaced in the circumferential direction and each of these injectors is treated as a "blade passage." The injectors penetrate 5.1 mm (6% span) from the casing into the flowfield (Fig. 1). They are 57 mm wide (12.9 deg of arc) and located at 1.75 rotor chord upstream of the rotor leading edge. Measurements by Suder et al. [1] indicated that the jet fills only 75% of the width of the injector. In this study the injection is modeled by source terms uniformly distributed over the injector face of 75%

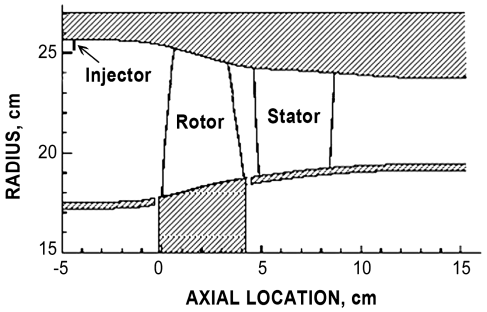

Fig. 1 High-speed single-stage axial compressor stage 35 (NASA rotor 35 and stator 37).

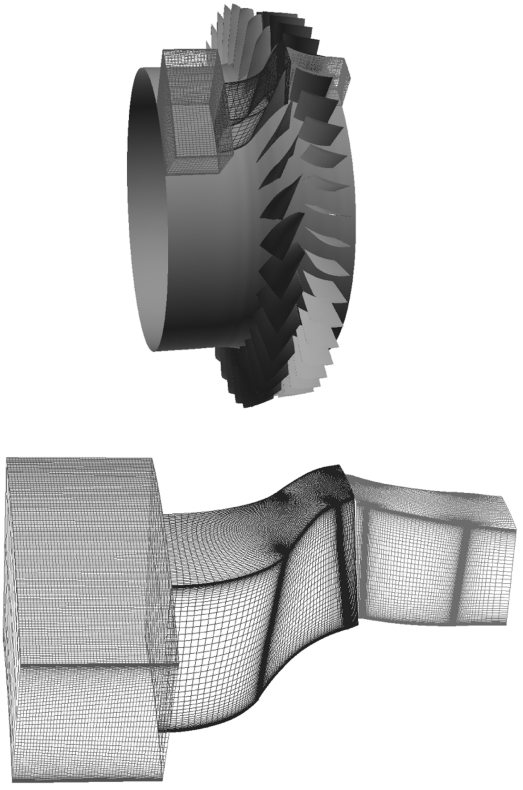

Fig. 2 Three-blade-row grid model for the stage 35 simulation.

width (10 deg arc). The injection model is identical to that of Hathaway and Strazisar [31] (also Suder et al. [1]) and has been shown to capture the essentials of the injection.

The grid size of each passage of the injector is $51(x)$, $71(r)$, and $166(\theta)$; the rotor is $151(x)$, $71(r)$, and $56(\theta)$ with $81(x)$ and $61(r)$ points on the blade; and the stator is $141(x)$, $71(r)$, and $79(\theta)$ with $81(x)$ and $53(r)$ points on the blade. The rotor tip clearance is 1% rotor tip chord. The grids are replicated around the annulus to generate a full-annulus grid with a total of 67 million points. The grid is then partitioned into 328 blocks that use 328 CPUs. The computation time is 24 h for one rotor revolution. In the simulation of the rotating spike, 10–30 revolutions were needed.

The numerical boundary conditions are briefly discussed here. At the inlet, an isentropic subsonic inflow condition is used, in which a radial profile of total pressure and total temperature is applied uniformly over the circumference. A time-accurate sliding interface is used to exchange flow information between blade rows. This interface allows unaltered pressure waves in all directions (axial, radial, and circumferential) to pass the blade rows. The tip gap is modeled using the model of Kirtley et al. [32]. This model conserves both mass and momentum through the tip gaps without the need of gridding the actual tip clearance gap. A gridding strategy suggested by Van Zante et al. [33] is adopted here, with 10 radial points in the tip

gap region. Although the detailed physics of the development of the leakage vortex are not captured, this tip clearance model was considered adequate for predicting the strength of the leakage vortex, its size, and direction [34].

At the exit, the traditional choice of radial equilibrium exit condition, in which a preset exit pressure level is frozen throughout the simulation, is not suitable for near-stall or during-stall conditions. This is because the exit pressure drops during stall and a preset exit pressure cannot match the drop. This problem is relieved by the use of a "choked" throttle model that specifies corrected mass flow at the exit.[¶] This boundary condition allows the variation of exit pressure through the specification of a corrected mass flow based on the evolving exit stagnation condition.

Constrained by the computational resources for the full-annulus simulations, the axial extent of the computation domain upstream and downstream of the stage is short, which prevents the development of modal instabilities. The present study is restricted to capturing events leading to the spike instabilities and how the inception of these spikes is impacted by tip injection.

IV. Stall/Control Simulations and Discussion

The stage is first run without tip injection to show the development of rotating spikes. This process is then repeated with the application of steady tip injection. The intent is to show sufficient evidence that the computational model reasonably captures representative behavior of compressors as they are throttled into stall rather than assuring that the model faithfully captures the exact operational characteristics of the tested compressor. It is fully recognized that some features of the flowfield of the simulated compressor are not captured by the current computation. For example, in this study the leakage gaps and actual blade geometry at the running condition may not be the same as the tested compressor. Also, the geometry of the upstream and downstream ducting is not included in the simulation. As a result, the computation is not expected to accurately predict the flowfield of the tested compressor, but rather to model the essential flow physics of compressor stall with and without tip-injection stall control. The underlying unsteady flow perturbations (e.g., modal waves, blade row interactions, manufacturing tolerances, vortex shedding, shock/vortex unsteadiness, etc.) that precipitate short wavelength "spike" instabilities that coalesce into stall cells are specific to every compressor. Although these features are relevant to predict how or when the actual test compressor stalls, they are not believed germane to understanding the fundamental spike inception stall characteristics of compression systems. In this study, the approach is to let the unstable flow develop without purposely introducing an artificial disturbance.

A. Stage 35 Without Injection

This simulation was undertaken to document the development of spike instability without the presence of tip injection. A detailed analysis of this result was reported in [17] and will not be repeated here. A compressor speed line at design speed is generated by incrementally decreasing the exit corrected mass flow. The comparison of the computed results with the experimental data is shown in Fig. 3. In this figure, for the no-injection case, point A is the last stable point and point B is a point which developed into a rotating spike.

The computed total-to-static pressure ratio is higher than the experiment with the largest discrepancy occurring at a mass flow of 20.3 kg/s where the computed value is 1.41, compared to the experimental data of 1.33. This discrepancy is likely caused by the modeling limitations as well as the differences between the geometry of the tested compressor and that which was simulated, as mentioned before. The computed no-injection speed line near the peak pressure (point A) has a negative slope and is similar to the experimental no-injection speed line. Because the focus of this study is on the characteristic features associated with spike inception, we judged the current simulation to be reasonable for this purpose.

[¶]Adamczyk, J. J., private communication, 2004.

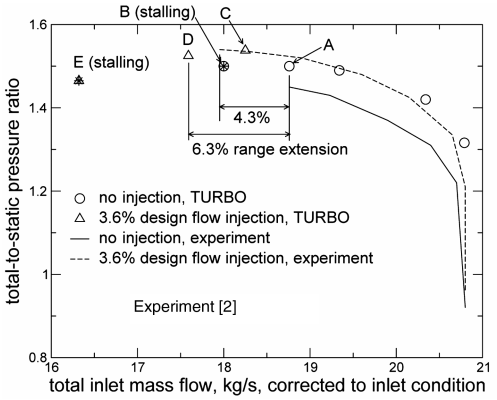

Fig. 3 Stage 35 predicted and measured performance.

In the simulation, eight numerical pressure probes were distributed around the circumference. The probes are located 44% chord upstream of the rotor leading edge at 98% span. They are arranged in 4 groups of 2 in order to fit outside the 12 injectors. The circumferential locations are 10, 70, 100, 160, 190, 250, 280, and 340 deg. These probes are fixed in space. Pressure time traces are shown in Fig. 4, in which the pressure level is offset by the probe circumferential location.

Small, but periodic pressure variations caused by the rotor blade passing can be seen in the first two revolutions of Fig. 4. The instability, identified as the larger disturbance on top of the periodic variation, first shows up at $t = 0.5T$ ($T =$ time for one rotor revolution). It then grows as it moves around the annulus with a speed indicated by the slope of the lines connecting the location of the disturbance at various probe locations. Initially the disturbance travels at 100% rotor speed. It then slows to 84% and eventually 43% in five revolutions as the compressor stalls.

In Fig. 5, the entropy on a surface of revolution near the casing is shown at $t = 3.8T$, the early phase of the development of the instability. The full-annulus surface is illustrated by two half-annulus surfaces. Three separate high entropy regions can be seen with the axial extent covering from one chord upstream to just aft of the leading edge of the stator. The evolution of the instability is similar to the spike stall inception in that localized, three-dimensional pockets of instability in multiple rotor passages erupt to first form small-sized multicell rotating spikes. These spikes initially travel at near rotor speed, merge, and slow to about half of the rotor speed [35].

B. Stage 35 with Injection

Tip injection is used in the present simulation to show improvement of the compressor operating range. The computed speed line with steady injection is compared to the experimental measurement in Fig. 3, where the total mass flow is the sum of the

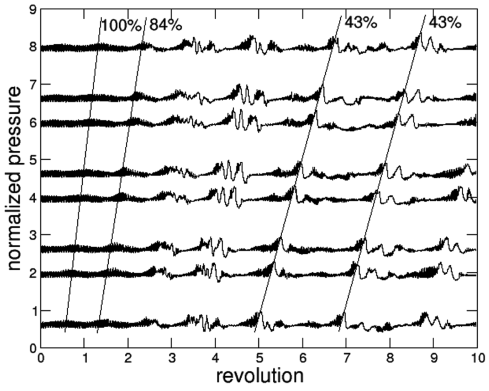

Fig. 4 Time history of static pressure variation at eight locations around the annulus located 44% chord ahead of the rotor of stage 35 without injection, point B.

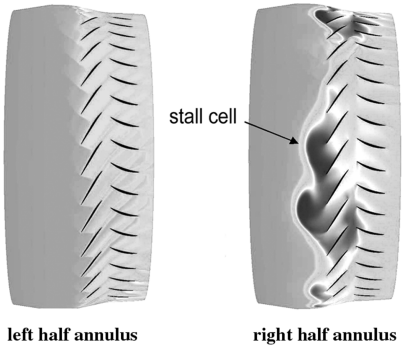

Fig. 5 Entropy of stage 35 without tip injection, corrected exit mass flow = 13.6 kg/s, $t = 3.8T$, point B.

inlet and injection flow, corrected to the inlet condition. Three points were computed for the injection case beyond which the no-injection case stalls. These are denoted by points C, D, and E. Each of the points used a steady, 3.6% design flow rate through the 12 injectors. The computed characteristic compares reasonably well with the data, with D being the last stable point. Comparing point A (without injection) and D (with injection), the simulation shows an improvement of 6.3% in the operating range, compared to 4.3% for the experiment.

To examine the effect of the tip injection on the unstable flow, the flowfields without injection (B) and with injection (C) are compared. These two points were run with the same throttle setting with the corrected exit mass flow set at 13.6 kg/s. Point B developed into stall but point C was stable. Excluding the regions of the low entropy injector flow the overall entropy level of the case with injection as shown in Fig. 6 is lower than that of the no-injection case in Fig. 5. More important, the high entropy regions associated with the rotating spike in the no-injection case of Fig. 5 no longer exist in Fig. 6. The tip injection effectively removes the rotating spike at this throttle setting.

C. Characteristic Features for Flows with Injection

The simulations with tip-injection flow control were analyzed to understand how tip injection affects the onset of stall. Three different operating points were run, one of which (point E) stalled, and two of which (points C and D) were stable. The throttle setting (corrected exit mass flow) is 13.6 kg/s for point C, 13.2 kg/s for point D, and 12.8 kg/s for point E. Point D was considered a stable case due to the fact that it ran for for 28 revolutions without dropping into stall. Point E stalled after 14 revolutions. Point D will be analyzed first to observe the general flow characteristics that hold true for both stable and unstable cases. This is followed by a discussion of point E on the general flow features at the onset of stall. The flow will be analyzed by the visualization of disturbance cells and two quantitative metrics diffusion factor and angle of attack. The three approaches are discussed in the following.

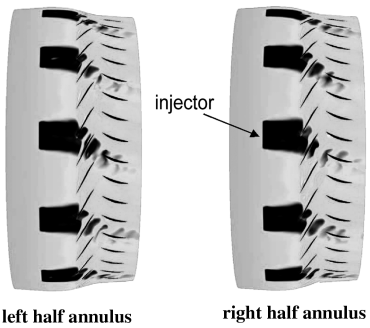

Fig. 6 Entropy of stage 35 with tip injection, corrected exit mass flow = 13.6 kg/s, point C.

1. *Disturbance Cell*

Because a stall flow relates closely to an axially reverse flow, an isosurface of zero axial velocity provides a useful means to construct three-dimensional representation of the stall cell. Several three-dimensional "pockets" are visualized in Fig. 7. These pockets are defined as the disturbance cells. Each of these cells is a closed volume composed entirely of negative axial flow. This can be seen clearly in Fig. 8 which shows the relative velocity vectors inside and outside a disturbance cell on a radial cutting plane. The disturbance cell is represented by the light-colored region. In this view, it is clear that all of the velocity vectors contained within the disturbance cell have a negative x component of velocity. The direction of the velocity vectors is also verified in Fig. 9, which is a relative velocity vector field near the suction side of the blade.

In addition to the negative x velocity shown in Fig. 8, this view shows that the relative velocity vectors have a positive radial component as well. This phenomenon will be discussed further in a later section. A great deal of circulation can be seen at the tip of the disturbance in Fig. 9, which reflects the instability (separation, swirling) in the flow surrounding the disturbance.

2. *Diffusion Factor*

The diffusion factor is a parameter used to indicate the magnitude of the adverse pressure gradient for a given airfoil/flow situation, as well as the amount of turning induced on the flow as it passes over the airfoil. The diffusion factor values were calculated as outlined by Hathaway and Strazisar in [31]:

$$\mathrm{DF} = 1.0 - \frac{W_{\mathrm{out}}}{W_{\mathrm{in}}} + \frac{\mathrm{abs}(R_{\mathrm{in}} * W_{t,\mathrm{in}} - R_{\mathrm{out}} * W_{t,\mathrm{out}})}{(R_{\mathrm{in}} + R_{\mathrm{out}}) * \sigma * W_{\mathrm{in}}} \tag{1}$$

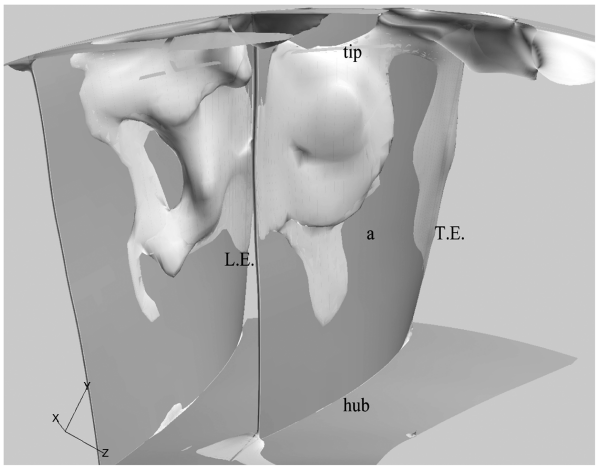

Fig. 7 Isosurface of zero axial velocity on suction surface of rotor blade a for point D. L.E. = leading edge; T.E. = trailing edge.

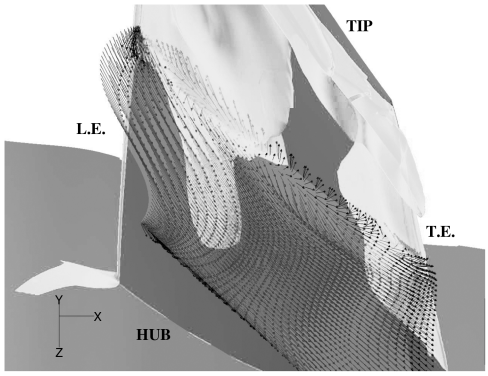

Fig. 8 Intersection of disturbance cell with radial-plane velocity vector surface at ~65% span, point D.

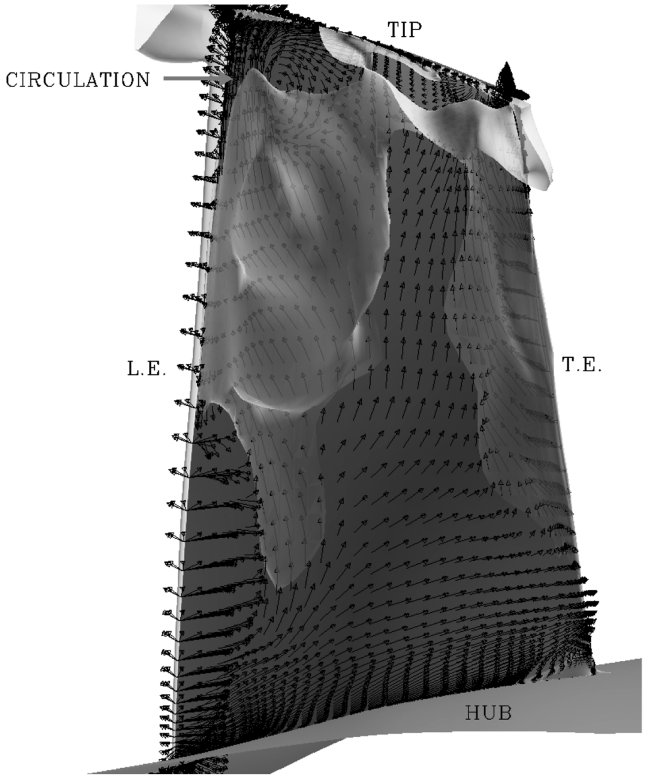

Fig. 9 Disturbance cell with relative velocity vector near the suction surface, point D.

where W_{in} and W_{out} are the mass-averaged inlet and outlet relative velocity magnitudes, respectively, R is the radial location of the point of interest, $W_{t,in}$ and $W_{t,out}$ are the inlet and outlet mass-averaged tangential velocity values, and σ is the solidity of the compressor. The inlet and outlet parameters are pitch-averaged values at axial locations of the blade leading edge and trailing edge, respectively.

The second term on the right-hand side of Eq. (1) reflects the outlet to inlet velocity ratio. The DF value goes up as this term gets smaller, indicating that the flow is diffusing. This would also reflect a stronger adverse pressure gradient as the flow travels along the length of the blade, which would increase the likelihood of boundary-layer separation. The last term in Eq. (1) reflects the change of angular momentum (turning) of the flow as it passes the airfoil. The more flow turning, the more work added to the flow, and consequently the higher the DF value would be, again increasing the likelihood of boundary-layer separation.

3. Angle of Attack

The angle of attack of the inlet flow to the blade was computed using the same data point distribution implemented for the diffusion factor analysis. Mass-averaged values were found in the same manner, with the angle of attack value for each point calculated as the difference between the flow angle of a given point and the stagger angle of the rotor blade at the same radial location. The idea behind choosing this particular metric was that the angle of attack should be a good indicator of the blade loading and thus the susceptibility of a given blade to boundary-layer separation.

D. Radial Migration of Disturbance Cells

As mentioned earlier, when investigating the direction of the velocity vectors within the disturbance cells, it was found that the vectors on the suction surface of the blades tended to have a positive radial component. This observation is consistent with the fact that the motion of the disturbance cells on the blades was, for the most part, moving downstream and radially outward. Figure 10 shows this phenomenon at four time steps. The interval of time between the figures corresponds to the time taken for the rotor to travel 0.4 rotor pitches. This figure shows the migration of the disturbance on the suction surface of one blade for the stable point D. The radial migration of the disturbance cells is also observed when the flow stalls.

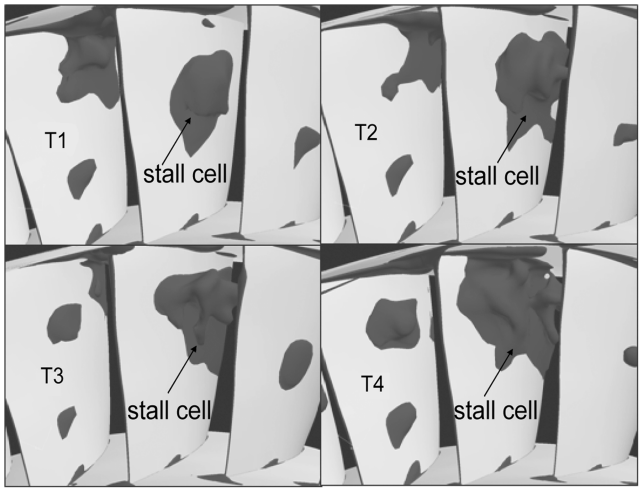

Fig. 10 Radial migration of the disturbance at 0.4 rotor pitch steps per frame in the rotor, point D.

The disturbance cell was initially quite small (T1), expanding as it moved toward the casing, resulting in a concentration of low-momentum flow on the casing (T4).

This radial motion is attributed to the radial, centrifugal force exerted on the fluid in the rotor due to the rotation. This force is present for the fluid both inside and outside of the disturbance cells. This is seen clearly in Fig. 9 as the vast majority of the relative velocity vectors have a strong radially outward component. Because the fluid within the disturbance cells would have a longer residence time in the passage than the flow outside of the disturbance cell, due to the low axial velocity, the centrifugal force would have a longer period to act upon it, forcing it to migrate to the casing. The expansion of the disturbance cells will be explained later.

E. Leading-Edge Spillage of Stall Flows

In the case that stalled, point E, it was found that the disturbances occupied the full circumferential breadth of the passages in the vicinity of the rotor tip when the simulation began to stall. This can be seen in the enclosed section in Fig. 11. This has been observed by Hathaway in unreported steady-state averaged passage simulations of several different compressor geometries both with various forms of tip injection and without. Inspection of when the rotor tip axial

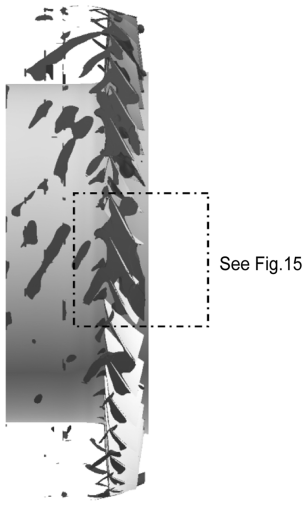

Fig. 11 Three-dimensional view of reverse flow pockets indicating spillage of disturbance, point E.

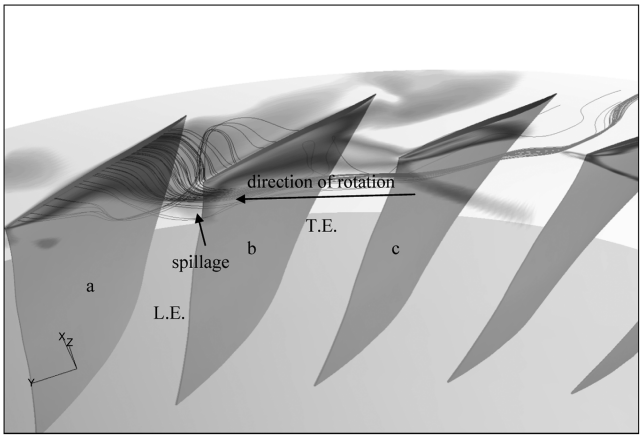

Fig. 12 Streamline view of disturbance spillage from upstream of rotor leading edge, point E.

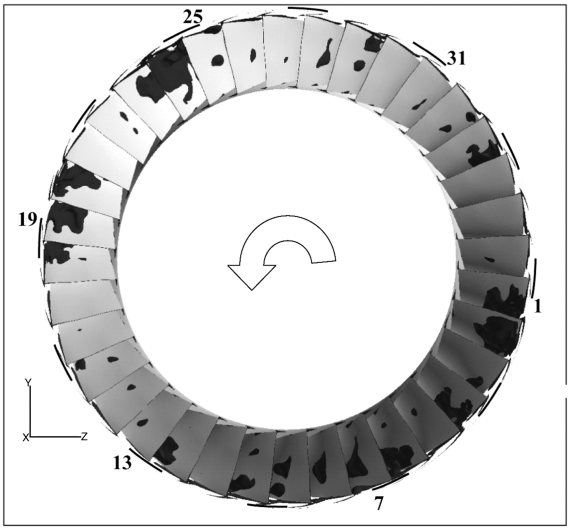

Fig. 13 Blade number references for diffusion factor and angle of attack figures (Figs. 14–19), point D.

velocity is less than or equal to zero across the rotor pitch as an indicator of incipient stall was first suggested by Adamczyk.** In addition, there was a great deal of spillage of the disturbances around the leading edge of the rotor blades. Figure 12 shows the spillage of the disturbances around the leading edge of the blades.

Because the velocity field of the transient flow evolves smoothly, streamlines match path lines well and were generated to track the particle movement. Figure 12 shows the streamlines of the flow in the vicinity of the tip along with the negative axial velocity contour (shaded dark) on a radial plane at the blade tip. The streamlines were seeded along the tip of the suction side of blade a. This view indicates that a great deal of the flow is spilling around not only the leading edge of the adjacent passage (blade b), but also around the leading edge of the next passage (blade c). This spillage is instigated by the presence of the reverse flow pockets. As the flow spills over the tip of blade a, it is swept upstream by the reverse flow present in the passage, which causes it to migrate forward of the leading edge of blade b. This increases the angle of attack of the flow in the vicinity of blade b and thus intensifies the disturbances. As it passes the leading edge of blade b, the reverse flow present in this passage once again pushes the flow upstream causing it to flow around the leading edge of blade c. This is continued until the flow enters a passage without a reverse flow pocket (that spans the entire pitch). The disturbance is then swept downstream. Within the passage in which the disturbance was initiated one observes that some of the flow is pulled downstream but is then reverted back upstream. This spillage allowed the disturbances in the individual blade passages to merge, which led to a slow down of the migration of the disturbance around the annulus.

The observed slow down could be due to the following hypothesis: As the disturbance cells merge, the size of the merged cell increases in both the axial and spanwise directions. Because the disturbance cell represents low-momentum flow with high inertia, the blades move through it as they would stagnant flow, causing the relative motion of the disturbance to be in the opposite direction of rotation, producing a slow down in the absolute frame.

F. Correlation Between Diffusion Factor, Angle of Attack, and Disturbance Cells for Stable Condition D

The instantaneous flowfield at point D, see Fig. 3, is examined in this section to study the flow characteristics for stall onset based on disturbance cells, angle of attack, and diffusion factor profiles. The results in Figs. 13–19 are separated into three groups, each corresponding to an identical position relative to the injectors. The passage numbers are identified in Fig. 13. The locations of the injectors are indicated by the black circumferential segments just outside the blade tips.

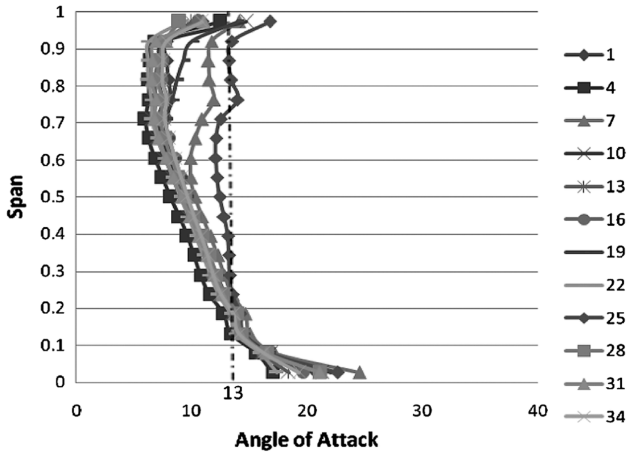

Fig. 14 Angle of attack values (point D) for blades 1, 4, 7,. . ., 34.

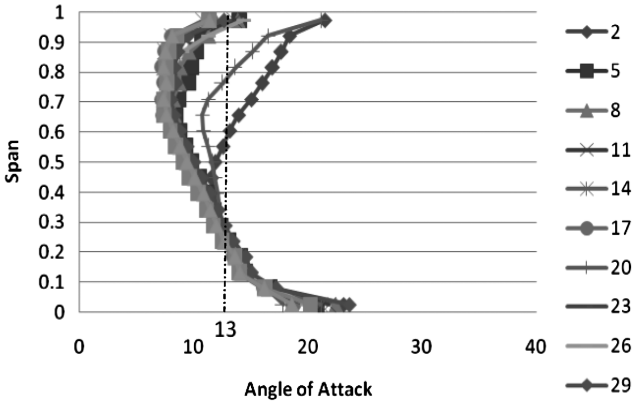

Fig. 15 Angle of attack values (point D) for blades 2, 5, 8,. . ., 29.

The simulation results show that there is a definite correlation between angle of attack and the evolution of disturbances. The plots for each of the passages exhibited almost identical angle of attack values from the hub to approximately 20% span. It is also clear that each passage exhibits a drastic increase in angle of attack above 90% span. The major differences between passages could be found from 20% span to the tip. Upon inspection of Fig. 13, it can be seen that on blades 2, 20, and 24 disturbance exists along their leading edge. This

**Adamczyk, J. J., private communication, 2000.

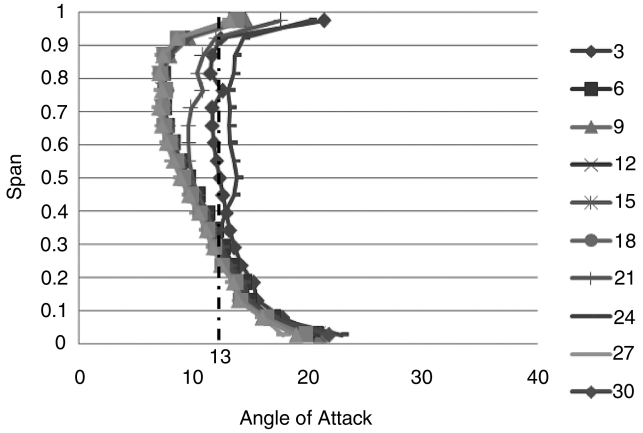

Fig. 16 Angle of attack values (point D) for blades 3, 6, 9,. . ., 30.

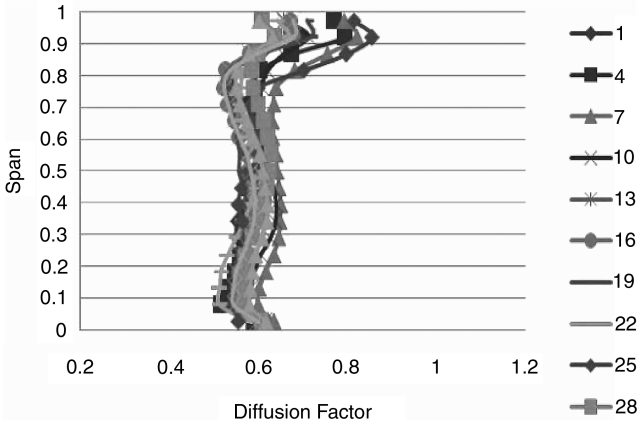

Fig. 17 Diffusion factor values (point D) for blades 1, 4, 7,. . ., 28.

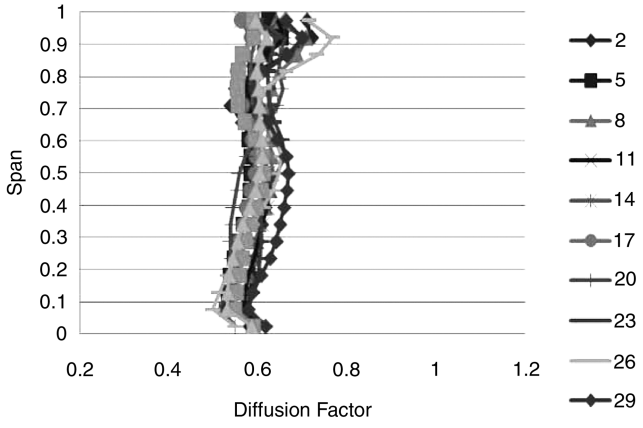

Fig. 18 Diffusion factor values (point D) for blades 2, 5, 8,. . ., 29.

is reflected in the angle of attack values in Figs. 15 and 16. It appears that if the angle of attack between midspan and 90% span attains a value greater than approximately 13 deg, leading-edge separation will occur.

Attempting to correlate diffusion factor with the presence of disturbances proved considerably more difficult than correlating angle of attack with the presence of disturbances. When looking at individual passages, there does not appear to be any significant correlation. The one useful result that came out of this attempt is that with tip injection (at operating point D in Fig. 3), for the vast majority of the blades there is an increase in magnitude of the diffusion factor in the vicinity of midspan. This is clearly seen by the annulus-averaged values in Fig. 20 where before stall (points C and D), the midspan diffusion factor with tip injection is 0.61. This lends

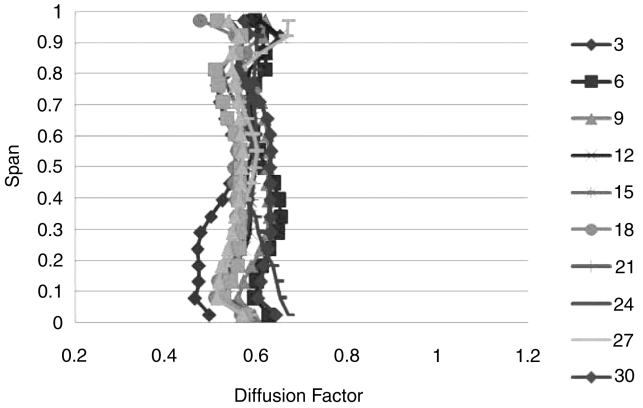

Fig. 19 Diffusion factor values (point D) for blades 3, 6, 9,. . ., 30.

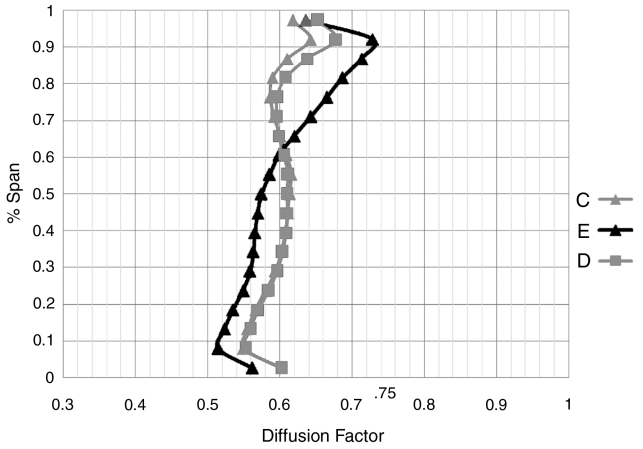

Fig. 20 Annulus-averaged diffusion factor distributions for three cases.

evidence to the fact that, for this simulation with tip injection suppressing tip stall, disturbances are generally formed in the midspan before migrating to the tip region. This would not be expected to occur for compressors wherein the midspan is lightly loaded, such as that without tip injection (operating point A in Fig. 3). Figure 20 indicates that the stable cases, C and D, had diffusion factor values which were lower in the tip region than that of the unstable, E case. The results suggest that a diffusion factor value somewhere between 0.68 and 0.73 in the tip region would indicate the appearance of a rotating spike.

Annulus-averaged angle of attack indicates that there is an increase in the overall angle of attack as stall is approached. From Fig. 21, it can be seen that the unstable, E case has higher values for the angle of attack across almost the entire span. This phenomenon is

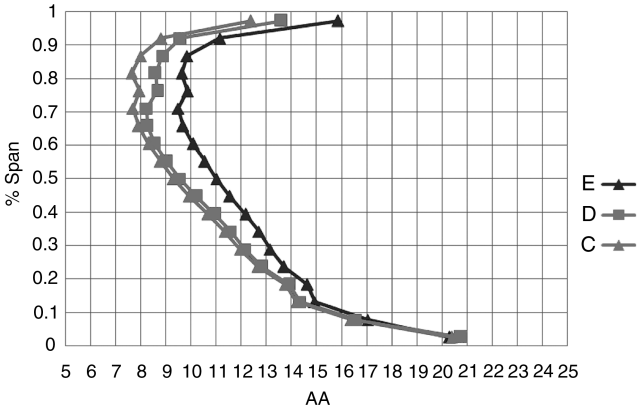

Fig. 21 Annulus-averaged angle of attack distribution for three cases.

consistent with the fact that the through-flow rate decreases as stall is approached. At 50% span, the stable cases (C and D) have values less than 9.5 deg. Using the conclusion from previous individual blade correlation, it is speculated that an averaged midspan angle of attack exceeding 9.5 deg would indicate the inevitability of instability. This indicator would assume that the production of disturbance flow which is prevalent in the midspan is one of the sources leading to the rotating spike.

The reason for an overall increase of angle of attack values in the tip region, besides the existence of reverse flow pockets, is that the boundary-layer flow on the casing creates an axial velocity deficit in the tip region, thereby reducing the axial component of the relative flow angle, increasing the angle of attack. This increase in angle of attack also helps explain the expansion of the disturbance cells as they migrate toward the tip: a higher angle of attack moves the boundary-layer separation point on the suction surface forward, increasing the magnitude of the disturbance cell that is already present by creating more separated/swirling flow.

With the general flow features identified in the previous section, the same analysis procedures are used to examine how tip injection mitigates instability onset. This will be done by comparing the results for stable point D to the results for unstable point E.

G. Stable Case (Point D)

The migration of the disturbances mentioned earlier lends a great deal of insight into the functioning of the tip-injection cases. The first characteristic of the stable case is that low-momentum flow migrates to and congregates in the tip region of the blade passages. The introduction of the tip injectors provides high-axial-momentum flow which alleviates the momentum deficit associated with the disturbance cells. A few snapshots are given in Fig. 22, each separated in time by the time it takes for the rotor to rotate through 0.8 of a rotor pitch.

The tip injectors are represented by the white streaks in the dark region above blade tips in Fig. 22. This sequence of snapshots is generated in the rotor frame where the injectors are seen moving over the blades in the direction opposite to rotor rotation. As blade a in the figure passes through one injector, the disturbance cell at midspan has almost disappeared, as can be seen by the difference between T3 and T4. The disturbance on blade b, however, does not get cleaned up after passage through only one injector. Its growth can be seen after it passes through one injector from T1 to T2 and it continues to grow from T2 to T3. The volume of the disturbance in the tip region is reduced somewhat every time it enters a region of tip injection. This can be seen at T1 and T4. A larger (by volume) disturbance, as seen on blade b could pass through multiple injectors, successively reducing the disturbance volume, before eventually being swept downstream. This was observed from animations of the unsteady results. The sweeping away of the disturbance is accomplished by the addition of high-energy flow into the tip region which also increases axial momentum in the tip region, thereby reducing the volume of the disturbance.

A second characteristic, which correlates with the first, is the increase and decrease in the intensity of disturbances which travel at rotor speed. This behavior is shown by the pressure traces of Fig. 23. Here, spikes of small disturbance persistently appear. At this operating point without the presence of tip injection, the rotor would drop into a rotating spike.

The life span of the disturbance is indicated in Fig. 23 by the length of the dashed lines. Most disturbances are short lived and disappear within one rotor revolution. All of them rotate at rotor speed. It demonstrates that the injection stabilizes the otherwise unstable flow, which, when left uncontrolled, will develop into a rotating spike.

H. Unstable Case (Point E)

Point E from Fig. 3 is unstable. This case ran for just under 14 revolutions before stalling as seen in Fig. 24. Figure 24 uses the same probes previously mentioned for Fig. 23. As with the stable case, disturbance cells were formed in the midspan of rotor blades which then migrated to the tip region of the rotor. Unlike the stable case, the disturbances in this case do not get swept downstream by the injected fluid. Instead, they continue to propagate for approximately 5 revolutions.

The initial disturbance mapped by the dashed line travels at rotor speed. A more dramatic disturbance developed during the ninth revolution. This disturbance travels at approximately 49% of rotor speed. This slow down is similar to the spike inception instability observed in the no-injection case.

The slow down of the disturbance seems to be directly related to the point at which it begins to occupy the entire pitch of a particular

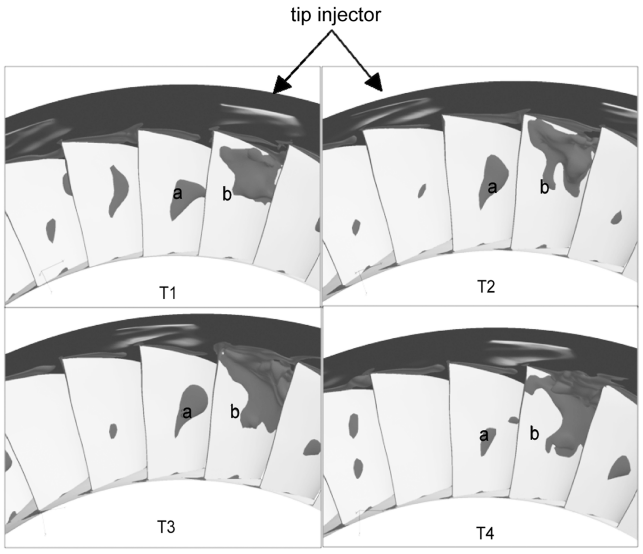

Fig. 22 Disturbance reduction through the steady injectors at 0.8 rotor pitch time increments per frame, point D.

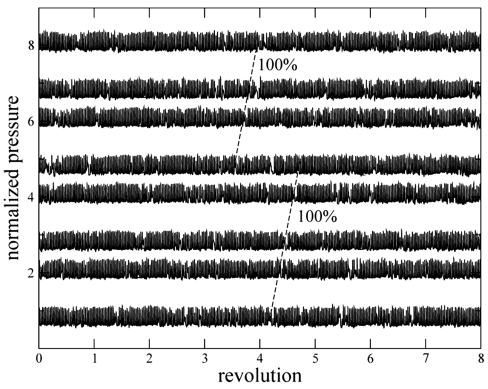

Fig. 23 Time history of entropy variation at eight locations around the annulus located 44% chord, point D.

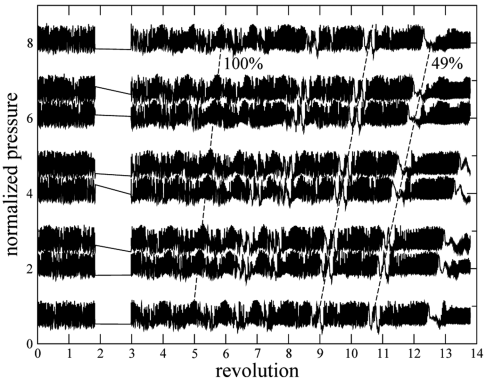

Fig. 24 Time history of pressure variation at eight locations around the annulus located 44% chord upstream of the rotor leading edge, point E.

rotor passage (Fig. 11). Upon this occurrence, the disturbance propagates upstream beyond the leading edge of the rotors. This allows it to migrate to the adjacent passage, merging with the disturbance already present in the adjacent passage. This process is continued until the volumetric magnitude of the disturbance cell (region of reverse flow) grows to such a size that the compressor can no longer support the required mass flow.

V. Conclusions

Unsteady full-annulus simulations of a high-speed axial compressor with and without tip-injection flow control have been conducted. Because the simulation does not model every aspect of the tested compressor, the conclusions made here may not be generic and are relevant only to the extent modeled by the simulation.

As the compressor throttles to stall without tip injection, the simulation shows that a disturbance first travels at the rotor speed. It then transitions to a spike disturbance of 84% rotor speed consisting of multiple disturbance cells. The disturbance eventually coalesces into a single rotating cell of 43% rotor speed. The simulation demonstrates that the code is able to simulate flow instabilities and their subsequent growth into a fully developed rotating spike disturbance. This simulation models the spike inception and instability growth process without the use of an artificial disturbance.

With tip injection present as the compressor is throttled beyond the noninjection stall point, the lower spans began to exceed their loading capability (high angle of attack and diffusion factor) resulting in local suction surface reverse flow pockets that centrifuged out to the rotor tip. As they migrate, their volume expands due to the increased angle of attack in the tip region. In the stable (sufficient injection) case, the disturbance cells would be washed away by the injectors. Some disturbance cells were swept downstream after passing through only one injector while others passed through multiple injectors before being swept downstream.

In the unstable (insufficient injection) case, the migration of the disturbance cells from lower spans to the tip region caused a buildup of reverse flow, due to the inability of the tip injection to offset the production of disturbance cells at this unstable flow point, to the point that the entire circumferential breadth of the passage would be within a disturbance cell. When this occurred, the disturbance cell would begin to spill into the adjacent passage. This would increase the overall size of the disturbance cell in both the axial and spanwise directions. The disturbance cell would then continue this migration around the annulus, absorbing the disturbance cells in the other blade passages as it traveled. This migration was reflected in a slow down in the speed at which the disturbance traveled around the rotor as observed in the absolute frame of reference.

In summary, it was shown that numerical simulations can provide valuable insight into the processes by which tip injection delays the onset of stall. Insight gained from the present study can be used to refine tip-injection control with the intent of reducing the amount of fluid injected to achieve a given increase in the stall margin.

Acknowledgments

This research was supported by the U.S. Army Research Office and The Advanced Virtual Engine Test Cell, Inc. We would like to thank the DoD Major Shared Resource Center, the Ohio Supercomputer Center, and the IBM Rochester Center for their generous allotment of computing time.

References

[1] Suder, K. L., Hathaway, M. D., Thorp, S. A., Strazisar, A. J., and Bright, M. M., "Compressor Stability Enhancement Using Discrete Tip Injection," *Journal of Turbomachinery*, Vol. 123, Jan. 2001, pp. 14–23. doi:10.1115/1.1330272

[2] Weigl, H. J., Paduano, J. D., Frechette, L. G., Epstein, A. H., Greitzer, E. M., Bright, M. M., and Strazisar, A. J., "Active Stabilization of Rotating Stall and Surge in a Transonic Single Stage Axial Compressor," *Journal of Turbomachinery*, Vol. 120, No. 4, 1998, pp. 625–636. doi:10.1115/1.2841772

[3] Spakovszky, Z. S., Weigl, H. J., Paduano, J. D., van Schalkwyk, C. M., Suder, K. L., and Bright, M. M., "Rotating Stall Control in a High-Speed Stage with Inlet Distortion: Part 1—Radial Distortion," *Journal of Turbomachinery*, Vol. 121, July 1999, pp. 510–516.

[4] Spakovszky, Z. S., van Schalkwyk, C. M., Weigl, H. J., Paduano, J. D., Suder, K. L., and Bright, M. M., "Rotating Stall Control in a High-Speed Stage with Inlet Distortion: Part 2—Circumferential Distortion," *Journal of Turbomachinery*, Vol. 121, July 1999, pp. 517–524.

[5] Strazisar, A. J., Bright, M. M., Thorp, S., Culley, D. E., and Suder, K. L., "Compressor Stall Control Through Endwall Recirculation," ASME Paper GT2004-54295, June 2004.

[6] Nie, C., Xu, G., Cheng, X., and Chen, J., "Micro Air Injection and Its Unsteady Response in a Low-Speed Axial Compressor," *Journal of Turbomachinery*, Vol. 124, Oct. 2002, pp. 572–579. doi:10.1115/1.1508383

[7] Day, I. J., "Stall Inception in Axial Flow Compressors," *Journal of Turbomachinery*, Vol. 115, 1993, pp. 1–9. doi:10.1115/1.2929209

[8] Hoying, D. A., Tan, C. S., Vo, H. D., and Greitzer, E. M., "Role of Blade Passage Flow Structures in Axial Compressor Rotating Stall Inception," *Journal of Turbomachinery*, Vol. 121, Oct. 1999, pp. 735–742.

[9] Vo, H. D., Tan, C. S., and Greitzer, E. M., "Criteria for Spike Initiated Rotating Stall," ASME Paper GT2005-68374, 2005.

[10] Davis, R. L., and Yao, J., "Prediction of Compressor Stage Performance from Choke Through Stall," *Journal of Propulsion and Power*, Vol. 22, No 3, 2006, pp. 550–557. doi:10.2514/1.15463

[11] Gong, Y., Tan, C. S., Gordon, K. A., and Greitzer, E. M., "A Computational Model for Short Wavelength Stall Inception and Development in Multistage Compressors," ASME Paper 98-GT-476, June 1998.

[12] Stein, A., Niazi, S., and Sankar, L. N., "Computational Analysis of Stall and Separation Control in Centrifugal Compressors," *Journal of Propulsion and Power*, Vol. 16, No. 1, 2000, pp. 65–71. doi:10.2514/2.5532

[13] Khaleghi, H., Boroomand, M., Teixeira, J. A., and Tousi, A. M., "A Numerical Study of the Effects on Injection Velocity on Stability Improvement in High-Speed Compressors," *Proceedings of the Institution of Mechanical Engineers. Part A, Journal of Power and Energy*, Vol. 222, No. 2, 2008, pp. 189–198. doi:10.1243/09576509JPE443

[14] He, L., "Computational Study of Rotating-Stall Inception in Axial Compressors," *Journal of Propulsion and Power*, Vol. 13, No. 1, 1997, pp. 31–38. doi:10.2514/2.5147

[15] Saxer-Felici, H. M., Saxer, A. P., Inderbitzin, A., and Gyarmathy, G., "Numerical and Experimental Study of Rotating Stall in an Axial Compressor Stage," *AIAA Journal*, Vol. 38, No. 7, July 2000, pp. 1132–1141. doi:10.2514/2.1106

[16] Chen, J. P., Webster, R. S., Hathaway, M. D., Herrick, G. P., and Skoch, G. J., "Numerical Simulation of Stall and Stall Control in Axial and Radial Compressors," AIAA Paper 2006-418, Jan. 2006.

[17] Chen, J. P., Hathaway, M. D., and Herrick, G. P., "Pre-Stall Behavior of a Transonic Axial Compressor Stage via Time-Accurate Numerical Simulation," *Journal of Turbomachinery*, Vol. 130, Oct. 2008, p. 041014. doi:10.1115/1.2812968

[18] Hah, C., Bergner, J., and Schiffer, H.-P., "Short Length-Scale Rotating Stall Inception in a Transonic Axial Compressor—Criteria and Mechanisms," ASME Paper GT2006-90045, May 2006.

[19] Chen, J. P., and Briley, W. R., "A Parallel Flow Solver for Unsteady Multiple Blade Row Turbomachinery Simulations," ASME Paper 2001-GT-348, June 2001.

[20] Chen, J. P., and Whitfield, D. L., "Navier-Stokes Calculations for the Unsteady Flowfield of Turbomachinery," AIAA Paper 93-0676, Jan. 1993.

[21] Adamczyk, J. J., Celestina, M., and Chen, J. P., "Wake-Induced Unsteady Flows: Their Impact on Rotor Performance and Wake Rectification," *Journal of Turbomachinery*, Vol. 118, Jan. 1996, pp. 88–95.

[22] Turner, M. G., "Multistage Turbine Simulations with Vortex-Blade Interaction," *Journal of Turbomachinery*, Vol. 118, Oct. 1996, pp. 643–653.

[23] Richman, M., and Fleeter, S., "Navier-Stokes Simulation of IGV-Rotor-Stator Interactions in a Transonic Compressor," AIAA Paper 2000-3379, 2000.

[24] Barter, J. W., Vitt, P. H., and Chen, J. P., "Interaction Effects in a Transonic Turbine Stage," ASME Paper 2000-GT-0376, May 2000.

[25] Van Zante, D. E., To, W., and Chen, J. P., "Blade Row Interaction Effects on the Performance of a Moderately Loaded NASA Transonic Compressor Stage," ASME Paper GT-2002-30575, 2002.
[26] Gorrell, S. E., Okiishi, T. H., and Copenhaver, W. W., "Stator-Rotor Interactions in a Transonic Compressor, Part 2: Description of a Loss Production Mechanism," *Journal of Turbomachinery*, Vol. 125, 2003, pp. 336–345. doi:10.1115/1.1540120
[27] Green, B. R., Barter, J. W., Haldeman, C. W., and Dunn, M. G., "Averaged and Time-Dependent Aerodynamics of a High Pressure Turbine Blade Tip Cavity and Stationary Shroud: Comparison of Computational and Experimental Results," *Journal of Turbomachinery*, Vol. 127, 2005, pp. 736–746. doi:10.1115/1.1934410
[28] Van de Wall, A., Breeze-Stringfellow, A., and Dailey, L., "Computational Investigation of Unsteady Flow Mechanisms in Compressors with Embedded Supersonic Rotors," ASME Paper GT2006-90633, 2006.
[29] Gorrell, S. E., Car, D., Puterbaugh, S. L., Estevadeordal, J., and Okiishi, T. H., "An Investigation of Wake-Shock Interactions in a Transonic Compressor with Digital Particle Image Velocimetry and Time-Accurate Computational Fluid Dynamics," *Journal of Turbomachinery*, Vol. 128, 2006, pp. 616–626. doi:10.1115/1.2220049
[30] Dear, C., and Chen, J. P., "A Computational Validation Study of Parallel TURBO for Rotor 35," AIAA Paper 2006-0420, 2006.
[31] Hathaway, M. D., and Strazisar, A. J., "Impact of Discrete Tip Injection on Stabilization of a Transonic Compressor Rotor," *21st Army Science Conference*, 15–17 June 1998.
[32] Kirtley, K. R., Beach, T. A., and Adamczyk, J. J., "Numerical Analysis of Secondary Flow in a Two-Stage Turbine," AIAA Paper 90-2356, 1990.
[33] Van Zante, D. E., Strazisar, A. J., Wood, J. R., Hathaway, M. D., and Okiishi, T. H., "Recommendations for Achieving Accurate Numerical Simulation of Tip Clearance Flows in Transonic Compressor Rotors," *Journal of Turbomachinery*, Vol. 122, Oct. 2000, pp. 733–742. doi:10.1115/1.1314609
[34] Chima, R. V., "Calculation of Tip Clearance Effects in a Transonic Compressor Rotor," *Journal of Turbomachinery*, Vol. 120, Jan. 1998, pp. 131–140.
[35] Cumpsty, N. A., "*Compressor Aerodynamics*," Krieger Publishing Co., Malabar, FL, 2004.

C. Tan
Associate Editor